Received: 15 February 2023 | Revised: 22 June 2023 | Accepted: 21 July 2023

DOI: 10.1002/pc.27613

RESEARCH ARTICLE

Polymer COMPOSITES WILEY

Thermally conductive polypropylene composites as corrosion-resistant materials for plate heat exchangers

Hendrik Kiepfer[1] | **Paul Stannek**[2] | **Marco Grundler**[2] | **Hans-Jörg Bart**[1]

[1]Laboratory of Reaction and Fluid Process Engineering, TU Kaiserslautern, Kaiserslautern, Germany

[2]Zentrum für BrennstoffzellenTechnik (ZBT) GmbH, Duisburg, Germany

Correspondence
Hans-Jörg Bart, Laboratory of Reaction and Fluid Process Engineering, TU Kaiserslautern, 67663 Kaiserslautern, Germany.
Email: bart@mv.uni-kl.de

Funding information
Allianz Industrie Forschung, Grant/Award Number: 20999 N/1

Abstract

The suitability of polypropylene-graphite composites as materials for corrugated heat exchanger plates is investigated, as the associated materials have low density (<2.3 g/cm^3) and excellent corrosion resistance at a comparatively low price. Therefore, custom-made polymer composite plates with a thickness of 1–2 mm and a filling degree of up to 80 wt% were evaluated for their thermal and mechanical suitability with regard to their use in plate heat exchangers. Three-point flexural tests show that the loading of polypropylene with graphite leads to mechanical properties that are suitable for the application of heat exchanger plates. The simulated maximum overpressure is greater than 7 bar. The thermal conductivity of the composites was increased by a factor of 20 compared to pure polypropylene, resulting in thermal conductivities of up to 2.74 W/mK. Considering the density differences between the developed composites and stainless steel, similar thermal performances over a wide range of process conditions are obtained. Moreover, the composites investigated have lower crystallization fouling susceptibility compared to stainless steel, which is attributed to the low surface free energies of approximately 25 mN/m. For calcium sulfate fouling, the fouling resistance on stainless steel exceeds that on the composite by 1.5 m^{2}K/kW after 60 h.

KEYWORDS

crystallization fouling, mechanical properties, plate heat exchanger, polypropylene graphite composites, surface properties

1 | INTRODUCTION

In view of the global climate targets, the demand for heat exchangers with high heat transfer efficiency, such as plate heat exchangers, is increasing.[1] Compared to shell and tube heat exchangers, plate heat exchangers (PHEs) offer several advantages as shown by many authors.[2,3] With PHEs higher heat recovery rates can be achieved at low temperature differences compared to tubular heat exchangers. In addition, due to the thin plates used, they have a lower weight than tubular heat exchangers which is also associated with lower material and production costs. Especially in the environment of corrosive liquids, much energy can be saved, since corrosion-resistant alloys are associated with energy-intensive production and high material costs.[4] The generation of highly

turbulent flows in PHEs also makes them less susceptible to fouling,[5] resulting in reduced oversizing and downtimes. Other efficiency improvements involve heat transfer enhancement techniques, such as the use of nanofluids, as pointed out in a comprehensive review by Zhang et al.[6]

Furthermore, major savings could be achieved by the use of materials whose fabrication is associated with low-energy consumption, like polymers.[7] The interest in polymeric materials for heat ex-changer applications has been driven by their light weight, chemical stability, and corrosion resistance.[8,9] Moreover, they generally possess good fouling resistance.[10] For a broader application of polymers in heat transfer applications it is essential to increase the otherwise low-thermal conductivity (usually in the range of 0.1–0.5 W/mK[9,11,12]). But numerous authors have already shown that the production of polymeric composites can largely compensate for this disadvantage.[13–15] However, the examinations are mostly of a fundamental nature and focus often on thermal management applications in batteries, automotive, electronics, and photovoltaic devices.[14–16] There are not many studies on polymer composites with respect to their use in heat exchangers and are mainly related to the production of polymer composite tubes for application in seawater desalination.[17,18] Studies of polymer composites for application in PHEs are rare. However, graphite impregnated with synthetic resin is meanwhile used by manufacturers, such as SGL Carbon, to produce graphite heat exchangers under the DIABON® brand. Although they are corrosion resistant, the high manufacturing and processing costs of these artificial graphite heat exchangers are a significant barrier to their widespread use. A cost-effective innovative approach based on natural graphite sheets has recently been proposed by Jamzad et al.[19] Although this approach also requires impregnation with resin and a realization of large heat exchangers with the presented technique seems to be unlikely. Evidence that polymer composites based on the feedstocks investigated in this study can achieve very high thermal conductivities of around 12 W/mK has already been demonstrated.[20] However, the stated approach was based on injection molding of sheets, which is associated with a significantly longer production time and thus higher costs.

A cost-effective approach suitable for mass production, such as the manufacture of extruded polymer composite plates with enhanced thermal conductivity does not exist. Therefore, recently developed extruded polypropylene-graphite composites are evaluated for their suitability in corrugated PHEs. This includes the investigation of mechanical stability, thermal performance, and susceptibility to fouling, since most heat exchangers are affected by fouling, which can cause a tremendous economic loss as it directly affects the initial cost, operating cost, and performance of the heat exchanger.[21,22]

2 | EXPERIMENTAL

2.1 | Materials and preparation

The conductive plate-type polymer composites being investigated are manufactured at the Hydrogen and Fuel Cell Center (ZBT GmbH, Duisburg). A two-step process was used to achieve homogeneous material properties of the heat exchanger plates.

In the first step, the highly filled graphite polymer composites are prepared in a twin-screw extruder, followed by homogeneous granulation of the compound in a mill to particle sizes of less than 4 mm. The co-rotating twin-screw extruder is a Rheomex PTW25p by Thermo Electron. Each screw has a diameter of 25 mm and a L/D ratio of 42. The extruder system contains a vacuum pump for degassing the melt during the process. Control of extruder heating and rotating is done by special software, which saves all process data such as melt temperature and torque. Raw materials are descended into the extruder by a gravimetry system by K-Tron, containing one gravimetry for polymers and two for filler materials. This system is controlled by independent software, which saves all process data and adjusts filler content fully automatically. Polymer is conveyed directly into the extruder's input zone; filler material is conveyed into a side feeder, which is a small double screw conveyor with variable drive. The side feeder conveys the filler into the extruder, where it is mixed with the molten polymer. Most compounds were produced with a mass flow rate of 5–10 kg/h. The mass flow had to be changed regarding different bulk densities and flow behavior of graphite types, for example, the compound with the expanded graphite had to be produced with 2 kg/h since its bulk density is very low with 0.15 g/cm^3 and a specific surface area of 23.3 m^2/g while the graphite used by default (G45) has a bulk density of 0.73 g/cm^3 and a specific surface area of 4.8 m^2/g.

After the granulation of the compound, the pellets are transferred to a single-screw extruder, which is the basis of the film extrusion line, representing the second manufacturing step. There, the compounds melt again and pass through a wide slot die (width 250 mm) with variable gap dimensions (0.2–25 mm) to a calendar.

In order to achieve the best possible properties of the manufactured materials with regard to their application in PHEs, all conceivable influencing factors were investigated and evaluated. In this context, the graphite content and the material thickness were investigated in addition to the polypropylene (PP) and graphite grades. In

addition, sandblasting as a post-treatment of the samples was used to further improve their properties. The naming of the developed composites is composed as follows: PP grade (e.g., C143)—filler content in wt% (e.g., 75)—thickness in mm (if relevant)—additional characteristic of the material. The additional characteristics include the use of expanded graphite particles (exp) and the sandblasting of the material surface (sb). The result may look like: C143-75-exp. If the graphite grade is not specified, graphite with a D90 value of 45 μm (90 wt% of the particles are smaller than 45 μm) is used. Moreover, the stainless steel AISI 316Ti (hereafter referred to as SS) as a standard material in corrosion-resistant apparatus design is used as a comparative material.

2.2 | Material characterization

A detailed knowledge of the material properties is required to develop a conceptual design of heat exchangers based on the investigated composite materials. These properties can be divided into three subareas: mechanical, thermal, and surface properties.

2.2.1 | Mechanical characterization

In order to evaluate the mechanical properties of the polymer composites three-point flexural tests were performed according to DIN EN ISO 178 using the Instron 5565 testing machine under variation of the material thickness. The flexural strengths, flexural modulus, and flexural strain at break were determined.

The three-point flexural test was complemented by a destructive pressure test. The set-up consists of a pressure-stable SS tube with an inner diameter of 70 mm into which a specimen can be fixed using a clamping ring. The closed chamber is then flooded with water at ambient temperature and the pressure on the sample to be tested is gradually increased until it bursts. The pressure is continuously recorded with the pressure transducer FDA 602 L (Ahlborn GmbH; accuracy: 1% of the final value). The pressure tests are used to verify whether the determined flexural strengths are representative to evaluate the stability of the materials in PHEs.

However, mechanical simulations are needed to enable this. These provide the correlation between maximum pressure and maximum stress in the material. The mechanical simulations are, therefore, used, first, to determine the maximum stress in the material from the measured burst pressure. Second, they are used to simulate the maximum stress occurring in a PHE at a given pressure. Overall, it is thus possible to estimate how pressure-stable the developed materials are in a PHE.

Static simulations with Ansys Mechanical were performed to evaluate the mechanical properties. The computational domain for the simulation of the compression tests was taken over unchanged. For the simulation of the stresses in the PHE, the domain was considerably reduced compared to a heat exchanger plate used in practical applications due to its size and complexity, as shown in Figure 1.

Already this reduced computational domain consists of at least 3.3 million elements. The mechanical simulation of a complete heat exchanger would require extreme computing resources. In contrast, experimental data would be preferable. A corrugated PHE with a chevron angle of 60° and a corrugation pitch of 4 mm was chosen as the model for the geometry. However, due to the symmetry of the structure, only a representative section was chosen (41 mm × 37 mm). This in turn requires two plates as domain. One serves as the end plate, which is assumed to be fixed in position. The other corresponds to an overflowed thermal plate, which can be loaded with a pressure (corresponding to a hydrodynamic pressure by the overflowing fluid). PP from the Ansys material library was selected as the material for the simulation, with the elastic modulus adjusted according to the three-point flexural tests carried out. For a worst-case scenario, the lowest measured elastic modulus was selected accordingly. The computational grids were created as unstructured grids due to the complexity of the PHE geometry. To achieve mesh independence, the maximum deformation of the materials in the simulation was set as a convergence criterion. The mesh is automatically and selectively refined by Ansys Mechanical until the convergence criterion is reached. The simulations were considered to be convergent as soon as the deformation changed by less than 4% in the iterative procedure.

2.2.2 | Thermal characterization

The measurement of the thermal diffusivities α of the specimens was performed using the Laser Flash Apparatus 457 (Netzsch) at 25°C. The sample to be analyzed is exposed to a laser flash from the bottom side and the time-dependent temperature increase on the opposite side is recorded by an infrared detector. By means of a mathematical model, the thermal diffusivity is determined, which, multiplied by the density ρ and the specific heat capacity c_p, results in the thermal conductivity k according to Equation (1).

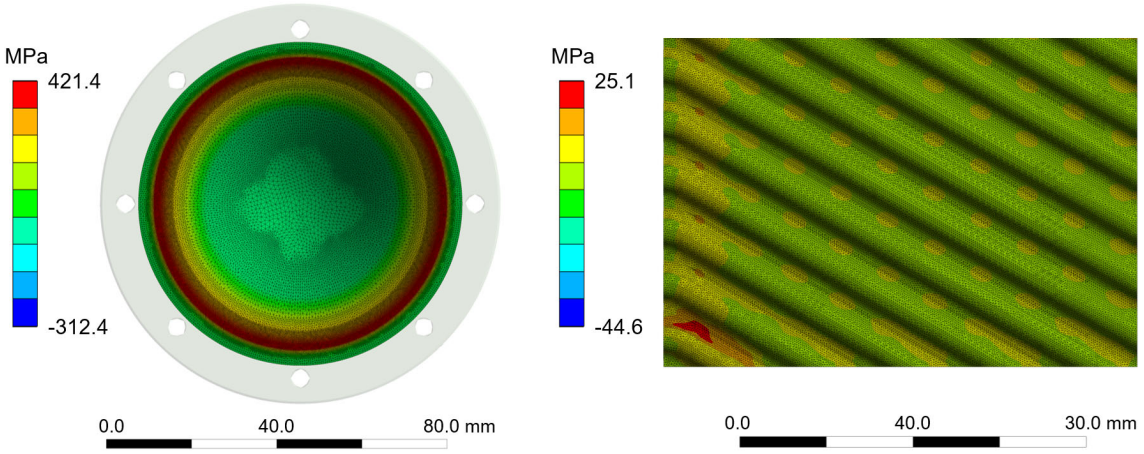

FIGURE 1 Computational domain and resulting stresses in the material at a load of 5 bar. (l) Pressure test set-up. (r) PHE section.

$$k = \rho \cdot c_p \cdot \alpha \tag{1}$$

The density of the samples was measured via a helium pycnometer. Since the determination of the specific heat capacities via the laser flash apparatus led to inaccuracies (the measurement is only carried out via a reference sample), these were determined by means of DSC measurements (DSC25 TA Instruments) at 25°C. However, the values of heat capacities and densities of classical polymers vary only slightly at room temperature. Therefore, thermal diffusivity is the most determining factor of the thermal conductivity of polymer composites.[22] For this reason, the heat capacities and densities were determined only from representative samples, that is, once for the respective polymers and different graphite mass fractions used.

2.2.3 | Surface characterization

The surface properties of materials have only a marginal influence on the performance of PHEs. However, they contribute significantly to fouling processes, which can greatly reduce the performance of heat exchangers during operation. For the interpretation and evaluation of the results of the fouling experiments, the knowledge of surface properties such as surface free energy and surface roughness is essential. Using a confocal microscope (μsurf Explorer, Nanofocus AG) 3D surface profiles are monitored from which various roughness parameters can be extracted and quantified according to EN ISO 25178. The mean arithmetic surface roughness is used to represent the topographic 3D characterizations since it contains more information compared to a 1D line roughness parameter. The surface free energies are determined according to the OWRK method[23,24] by measuring static contact angles. This method requires knowledge of contact angles of at least two liquids with known polar and disperse fractions of surface tension on the sample investigated. To ensure high accuracy of the determined surface free energies, static contact angle measurements with four reference liquids with different polarities (deionized water, ethylene glycol, dimethyl sulfoxide, and diiodomethane) were performed with an OCA 15 EC setup (Dataphysics).

2.3 | Plate heat exchanger modeling

To evaluate the performance of heat exchangers, the knowledge of the thermal conductivity λ and thickness of the separating walls s used is not sufficient. Finally, it is the overall heat transfer coefficient U or the transferred heat flux Q that is of relevance. To benchmark the performance of the polymer composites with SS, a model was set up to describe heat transfer in PHEs, as a function of the relevant parameters (thermal conductivity, wall thickness, mass flows $\dot{m}$, etc.). Considering the energy balance of a small control volume dx in the PHE according to Figure 2 and assuming that the heat transferred to the fluid from the adjacent channels is equal to the enthalpy change of the fluid, the following differential equations (1)–(3) are obtained to describe the temperature variation in the x-direction.

Here, Equation (1) corresponds to the first, Equation (2) to an intermediate, and Equation (3) to the last channel:

$$\frac{dT_1}{dx} = \frac{Uw}{C_1}(T_1 - T_2) \tag{1}$$

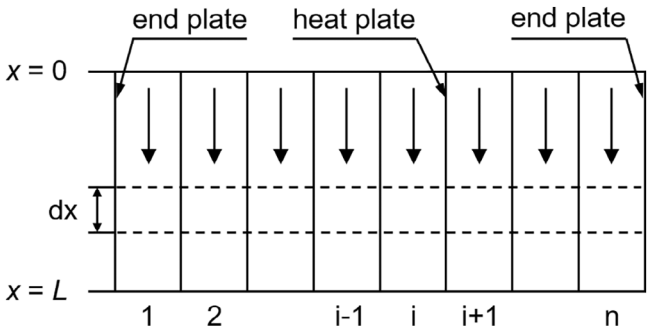

FIGURE 2 Schematic diagram of a PHE.

$$\frac{dT_i}{dx} = \frac{Uw}{C_i}(2T_i - T_{i-1} - T_{i+1}) \tag{2}$$

$$\frac{dT_n}{dx} = \frac{Uw}{C_n}(T_n - T_{n-1}) \tag{3}$$

with the overall heat transfer coefficient defined as:

$$U = \left(\frac{1}{h_h} + \frac{s}{k} + \frac{1}{h_c}\right)^{-1} \tag{4}$$

In the above equations, w is the effective plate width, and C is the heat capacity flow rate. The subscripts h and c indicate the hot and cold fluid stream. Thereby U and the fluid temperatures are solved as a function of the position x for higher accuracy instead of assuming an average overall heat transfer coefficient. In order to calculate the overall heat transfer coefficient U (Equation 4), respectively the convective heat transfer coefficients h, the Nusselt correlation according to Wanniarachchi et al.[25] was applied, as it covers a large range of Reynolds number ($1 \leq \mathrm{Re} \leq 10^4$, see Equations (5)–(8)).

$$\mathrm{Nu} = \left[\mathrm{Nu}_1^3 + \mathrm{Nu}_t^3\right]^{1/3} \mathrm{Pr}^{1/3} (\mu/\mu_w)^{0.17} \tag{5}$$

$$\mathrm{Nu}_1 = 3.65[\beta]^{-0.455}[\phi]^{0.661}\,\mathrm{Re}^{0.339} \tag{6}$$

$$\mathrm{Nu}_t = 12.6[\beta]^{-1.142}[\phi]^{1-m}\,\mathrm{Re}^{m} \tag{7}$$

$$m = 0.646 + 0.001[\beta] \tag{8}$$

With the geometry parameters β and Φ as described in Table 1. Since the fluid viscosity μ at wall temperature must also be known for the calculation of h with the above correlation, these are calculated according to the relation shown in Equation (9).

TABLE 1 Parameters of the PHE modeling.

Design parameter	Value
Effective heat exchanger width (w)	0.2 m
Effective heat exchanger length (L)	0.6 m
Chevron angle (β)	60°
Corrugation pitch (P)	8 mm
Corrugation amplitude (a)	1 mm
Enlargement factor (Φ)	1.15

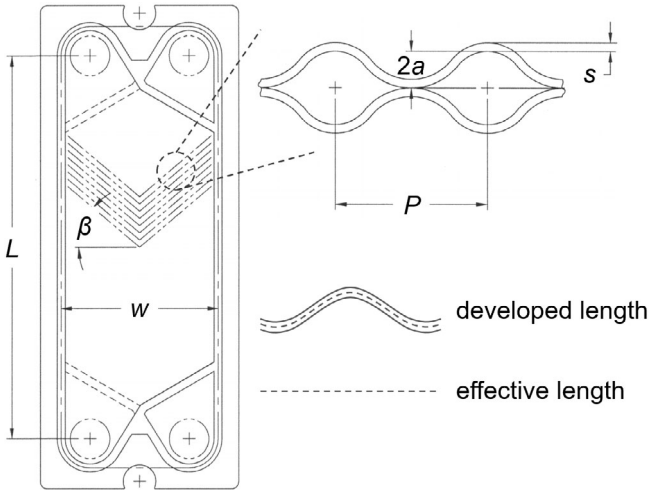

FIGURE 3 Design parameters of a chevron plate heat exchanger.

$$\dot{Q} = \frac{T_h - T_{w,h}}{\frac{1}{h_h A}} = \frac{T_{w,c} - T_c}{\frac{1}{h_c A}} = \frac{T_h - T_c}{\frac{1}{UA}} \tag{9}$$

where the subscript w indicates the temperature at the wall. Furthermore, various geometry parameters are included in the correlation or needed for the Equations (1)–(3). These were kept within the range of common practice as given in Table 1 and illustrated in Figure 3.

Thereby, the enlargement factor Φ represents the ratio between developed and effective length and is thus a function of corrugation amplitude and pitch. Finally, the heat transfer rate can be calculated via the temperature profiles and U can be given as a mean value for performance evaluation.

2.4 | Fouling test setup

The fouling experiments were carried out with different materials and operating conditions in the screening apparatus shown schematically in Figure 4. The set-up

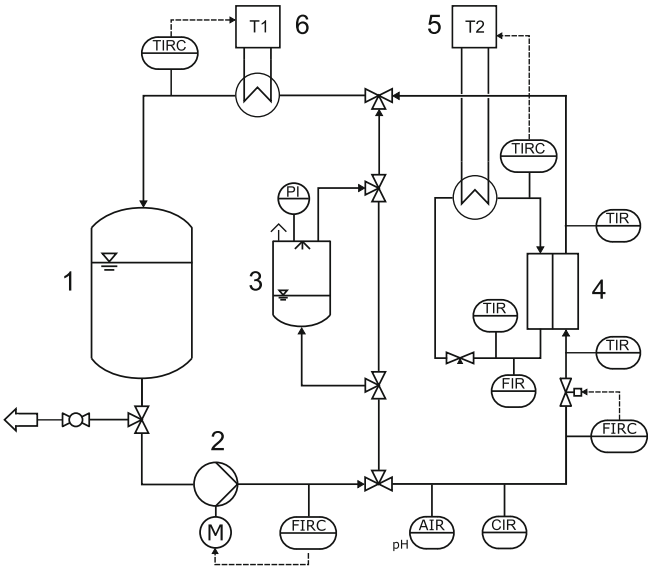

FIGURE 4 Process flow chart of the fouling screening apparatus. (1) Storage tank, (2) pump, (3) degasser, (4) heat exchanger, (5) heating circuit thermostat, (6) thermostat for bulk temperature control.

contains a vertically oriented heat exchanger test cell (4 in Figure 4) with a rectangular heat transfer surface of 144 cm^2, operated in counter-current flow. To avoid vortex formation and thus locally strong shear forces during the fouling experiments, the inlets are aligned longitudinally to the heat transfer surface. In addition, flow diffusers are located at the inlets and outlets to ensure a uniform flow over the heat transfer surface. However, the flow entering the heat exchanger test cell can neither be assumed as hydrodynamically nor thermally fully developed.

The sample material (the investigated polymer composites or SS) acts as a heat transfer wall and separates the cold liquid (salt solution) from the hot liquid (hot water). The heating side of the test section is made of polyoxymethylene and is additionally insulated to ensure adiabatic conditions. The solution side is made of polymethylmethacrylate to allow visual monitoring of the fouling process. Temperature sensors (Pt100 1/3 DIN) were placed in the flow directly at the inlet and outlet of the test sections, where the temperature distribution and flow profiles are homogeneous. The volume flow rates of the fluids entering the heat exchanger, as well as their temperature, are controlled for constant test conditions. All relevant temperatures and volume flows are recorded continuously to guarantee an accurate energy balance.

Using the energy balance for the calculation of the heat transfer rate, the overall heat transfer coefficient is calculated according to Equation (10). The calculations of the heat transfer rate refer to the cold fluid, where energy losses are almost excluded, as there is only a small temperature difference to the environment (approx. 15°C). Additionally, a very accurate Coriolis flow meter is used (measurement accuracy of 0.1%).

$$U = \frac{\dot{Q}}{A \Delta T_{lm}} \tag{10}$$

As a result of crystallization fouling, the heat transfer rate changes with increasing test duration, providing a transient overall heat transfer coefficient U_f. The resulting thermal fouling resistance R_f is then calculated according to Equation (11) referring to the initial overall heat transfer coefficient U_0 of the clean surface.

$$R_f = \frac{1}{U_f} - \frac{1}{U_0} \tag{11}$$

Prior to each experiment, the investigated polymer compound samples respectively the SS samples were cleaned with isopropanol and deionized water. The screening apparatus was cleaned several times with deionized water to ensure that there were no foreign ions left in the system. Calcium carbonate and calcium sulfate were chosen as model salts for the crystallization fouling mechanism. Both are inversely soluble salts which consequently deposit better on hot surfaces. Therefore, the fouling-causing salts were added to the cold bulk flow of pure deionized water at the start of the experiments. The feed solution for the $CaCO_3$ scaling tests is prepared by adding $CaCl_2 \cdot 2H_2O$ and $NaHCO_3$ to temperature-controlled deionized water. For $CaSO_4$ scaling, a similar procedure is conducted with the salts Na_2SO_4 and $Ca(NO_3)_2 \cdot 4H_2O$. Regarding the measurement of the initial overall heat transfer coefficients, the data were recorded for 15 min after reaching a steady state before the addition of the second salt (fouling is excluded until the second salt is added). The test period of the investigations was either adjusted to allow a sound conclusion on the fouling kinetics or to monitor an asymptotic fouling resistance. To accelerate the fouling processes, which can be achieved by higher wall temperatures, laminar flow conditions were created on the cold fluid side (which contains the fouling salts) and turbulent flow conditions on the hot fluid side. To prevent possible bubble formation on the surfaces (due to gas supersaturation), which would influence the fouling process, the bulk liquid was degassed before each fouling experiment with a vacuum spray-tube degasser (3 in Figure 4). According to the manufacturer, this should remove 90% of the dissolved gases. This procedure completely suppressed the formation of bubbles on the surface.

3 | RESULTS AND DISCUSSION

3.1 | Mechanical stability

Pure PP is not perfectly suitable for use in PHEs because of its low-thermal conductivity, acting as an insulator, but also because of its mechanical properties, like the high ductility (at least at temperatures above the glass transition temperature of max. 0°C). The high elongation at break of at least 50%[26,27] could lead to a displacement and blocking of channels and consequently to flow maldistributions and a performance loss when operating PHEs in the presence of high-pressure differences. However, due to its good mechanical (higher strength at lower densities compared to polyethylene) and thermal stability (up to 100°C long term[26]) compared to other commodity plastics, it represents a sound and cost-effective polymer matrix for composite materials for heat exchangers. The production of composites based on PP and graphite not only increases the thermal conductivity but also leads to an improvement in the mechanical properties, which makes the use in PHEs conceivable. Thus, as shown in Figure 5, the flexural modulus increases to at least 7.6 GPa, with a tendency for lower material thicknesses to result in higher flexural moduli. For comparison, the pure PP used has a flexural modulus of 1.4 GPa. This increase in the flexural modulus is also accompanied by an extreme reduction in elongation at break. In the case of the composite shown in Figure 5, the elongation at break is reduced from 700% (according to the datasheet) to max. 0.97%. Since the investigated materials are extruded, slightly different material properties are obtained in the extrusion and orthogonal to the extrusion direction. However, here only the worst results are shown (in the case of Figure 5 orthogonal to the extrusion direction).

In contrast to pure PP, distortion of the channels can thus be excluded when the materials investigated are used in PHEs, but mechanical failure during operation cannot. Whether the measured flexural strengths of 47–63 MPa are sufficient for the targeted application has to be determined experimentally or by simulation. At first glance, low wall thicknesses seem to be advantageous due to the higher flexural strengths. If the plates are thinner extruded, the graphite particles become more stretched, which could lead to the observed better mechanical stability. Thinner wall thicknesses in the heat exchanger would in turn have a positive effect on its performance due to a lower thermal resistance. However, the increase in flexural strength is not sufficient to compensate for the advantage of larger wall thicknesses. This can be concluded from Figure 6, showing the burst

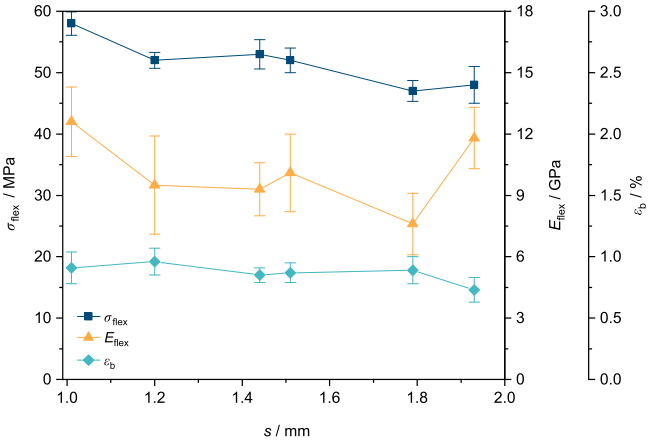

FIGURE 5 Flexural modulus, flexural strength, and flexural strain at break as a function of the thickness of C143-75. Measurement orthogonally to the extrusion direction.

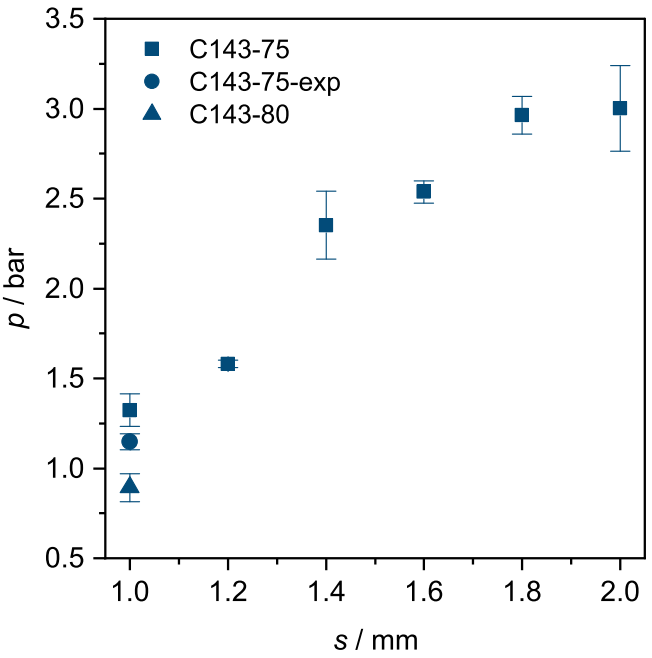

FIGURE 6 Burst pressures of the polymer composites.

pressures measured in the pressure test set-up as a function of wall thickness for the same material (C143-75). Consequently, an increase in wall thickness leads to a linear increase in burst pressure. By doubling the wall thickness from 1 to 2 mm, the burst pressure can be increased from 1.3 to 3 bar for the ideal setup. Furthermore, Figure 6 shows the influence of a variation in the graphite content or graphite grade. It was observed that the mechanical stability of the composites increases up to a filling level of 75 wt%, but drops steeply thereafter. The same applies to the use of expanded graphite particles, although the influence appears to be lower here.

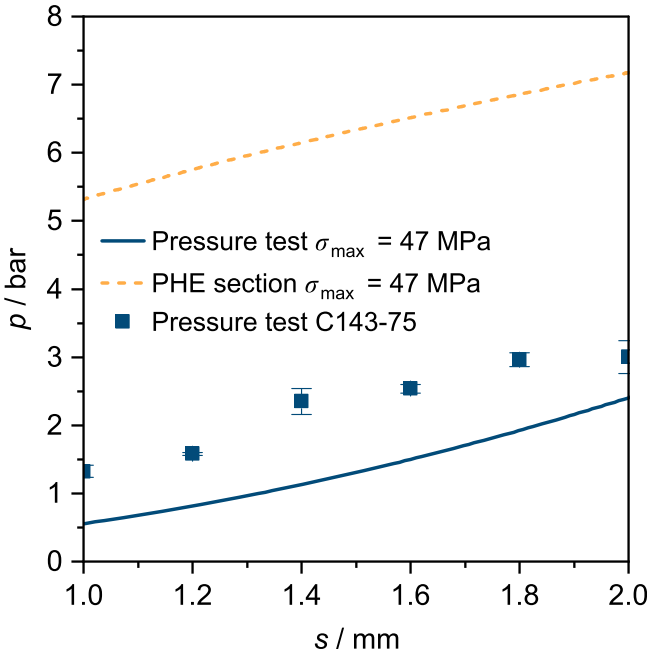

FIGURE 7 Worst-case material failure load for different material thicknesses and geometries.

In order to verify whether the results of the three-point flexural test and the burst pressure test are consistent, mechanical simulations were carried out. These provide a correlation between applied load and resulting mechanical stress in the material. For the final evaluation, a material failure theory suitable for the material must be used in the simulations. Since the materials are brittle (elongation at break less than 1%), the maximum principal stress is used as a criterion for material failure. The resulting maximum stresses in the material that lead to the bursting of the specimens vary according to the simulations between 103 and 58 MPa. The results are therefore only partially within the range of the measurements of the three-point flexural test. Here, the trend of greater strength at break with decreasing wall thickness is also much more pronounced. Thus, the specimens with 1 mm wall thickness broke on average at 103 MPa and with 2 mm wall thickness on average at 58 MPa. Nevertheless, the results of the three-point flexural test can be reliably used as a worst-case scenario (see Figure 7) for more realistic geometries, that is, of a PHE section (see Figure 1). Consequently, material failure is not expected before a maximum stress of 47 MPa is reached. Figure 1 shows that this criterion can be satisfied for a wide range of pressure loads, depending on the geometry. For a pressure load of 5 bar and a material thickness of 1 mm, the PHX would resist, whereas the specimen would have to fail in the burst pressure test already.

For a better understanding, Figure 7 shows the loadings that would lead to material failure according to the proposed condition ($\sigma_{max} = 47$ MPa) as a function of the wall thickness. It is clear that the local geometry can lead to a decisive contribution to the material stability in the final application. For example, the material under investigation would have to withstand pressures of more than 5 bar even at low wall thicknesses of 1 mm. The reason for this lies in the angled corrugations of PHEs. At minimum plate spacing, separate wave peaks of adjacent plates come in mutual contact. As a result, contact points occur, leading to stabilization. This can also be seen in the visualization of the stresses in the material (Figure 1). At the contact points, stronger loads occur in the material, which reduces the load on the surrounding areas. However, the strongest stresses in the material occur at the edges. The actual edges of the thermal plates, where the screw connections are located, are not explicitly considered here. On the other hand, the material could withstand even higher pressures in reality, since firstly a worst-case scenario is considered and secondly the maximum stresses in the material occur only in discrete elements of the computational grid and not over large areas. It is possible that the maximum stresses, which are locally limited to very small areas, are not sufficient for a material failure.

In order to put this into a correct perspective it must be added that the simulations alone are not sufficient for the dimensioning of PHEs with the materials examined in this study. The first reason is that, as explained earlier, not the complete geometry was considered. The second reason is that only experiments and simulations at ambient temperature were carried out. However, polymers in particular have mechanical properties that are strongly dependent on temperature. At the temperature studied, for example, they may tend to brittle failure (fracture), but at higher temperatures, they may tend to ductile failure (yield). Overall, representative experiments with the PP-graphite composites over a wide range of operating conditions thus remain to be conducted. To provide a brief classification of the state of the art, the simulated worst-case material loads are used as a basis. The maximum operating pressure of gasketed PHEs is limited to 20.4 bar.[28] With wall thicknesses of 2 mm overpressures of over 7 bar could be realized. This would probably cover a significant number of applications. An approach to further increase the mechanical stability would be to reinforce the composites with short carbon fibers. Kada et al.[29] were able to increase the tensile strength of PP composites with a comparatively low loading of carbon fibers (30 wt%) by 168% compared to pure PP. Of course, it should also be noted here that both process fluids usually flow into the heat exchanger at an overpressure. The highest relative pressure is therefore decisive.

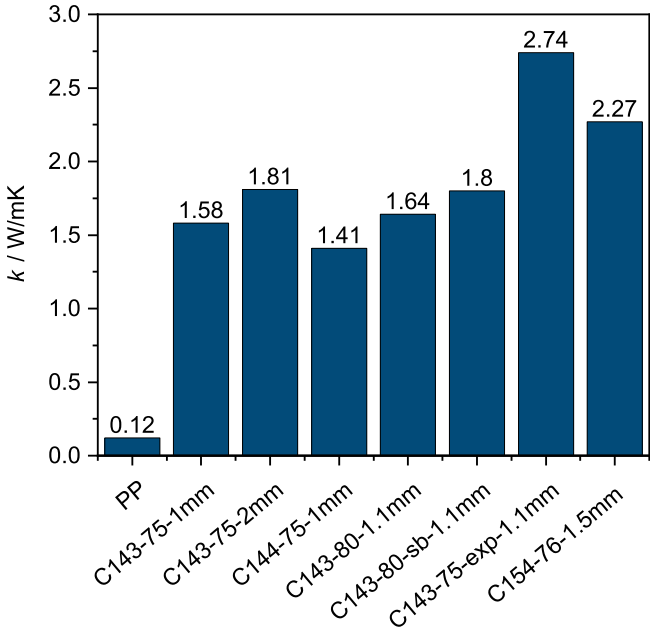

FIGURE 8 Through-plane thermal conductivities of PP composites and pure PP.[30]

3.2 | Thermal performance

The performance characteristics of a heat exchanger are usually indicated by the overall heat transfer coefficient U (see Equation 4) or UA, the overall heat transfer coefficient multiplied by the heat exchanging surface. The thermal resistances limiting U are the convective heat transfer coefficients h and the wall thickness and thermal conductivity of the heat transferring wall. In a material comparison, mainly the latter is important. The wall thickness of thermal plates in PHEs is usually in the range of 0.4 and 1.2 mm.[30] As shown in the previous section, smaller wall thicknesses are not feasible with regard to PP-graphite PHEs. On the contrary, wall thicknesses are more likely to be in the upper application range. Pure PP is, therefore, completely excluded for use in PHEs, not only because of its mechanical properties. With the thermal conductivity of PP (see Figure 8), a wall thickness of 1.2 mm results in maximum U values of 100 W/m^2 K. Metallic PHEs, in contrast, can achieve U values up to 7500 W/m^2 K. However, the production of PP-graphite composites has increased the thermal conductivity of the materials up to about 2300% (see Figure 8). Here, the greatest effect on thermal conductivity is achieved by using expanded graphite particles. Further positive properties on the thermal conductivity of the composites produced are a higher wall thickness and an increase in the graphite content, whereby at 80 wt% the manufacturing limit was almost reached. The PP grade used has only a very slight influence on the thermal conductivity of the composites. The use of polyethylene (C154) leads to a significant improvement in thermal conductivity (due to the higher thermal conductivity of polyethylene compared to PP), although it should not be considered because of the poorer mechanical properties. Interesting non-self-explanatory results are the increase of thermal conductivity by sandblasting of the surfaces and an increase in wall thickness. Due to the anisotropic character of the used graphite particles, the graphite-based PP composites are also anisotropic materials. The graphite particles are oriented in-plane by extrusion, which leads to much higher thermal conductivities in-plane compared to the through-plane thermal conductivity, which is relevant for heat transfer. A result that has already been described in a previous publication[31] and by other authors.[22] Thereby, the degree of stretching or particle orientation depends on the manufactured wall thickness. Unfortunately, the particles cannot be oriented in-plane without simple means. Approaches are the orientation of the diamagnetic graphite particles by means of strong magnetic fields,[32] which, however, would negate the cost advantage of the otherwise so inexpensive materials and production. The most promising alternative to obtain high thermal conductivities would be to process the compounds by injection molding. Thus, more thermal pathways are formed in the through-plane direction compared to sheet extrusion, resulting in high thermal conductivities,[20,22,31] but at the cost of increased production time.

By sandblasting the surfaces, the thermal conductivity (through-plane) can in turn be easily increased by a factor of 10%. After manufacturing, the materials have a thin polymer layer on the surface, which has a lower thermal conductivity than the core. Sandblasting removes this layer, which increases the overall thermal conductivity.

Summing up, a theoretical maximum U value of 2280 W/m^2 K is attainable with these materials. Although this value does not equal that of metallic PHEs, alloys with similar corrosion resistance properties to those of the composites studied should be used for comparison, for example, SS, whose thermal conductivity is not exceptionally high either (15 W/mK). In addition, these alloys have a density many times higher than the PP-graphite composites. If this is taken into account, much higher heat transfer areas can be achieved with the same heat transfer masses, which does not affect the U value, but the heat transfer rate positively. The density of SS, for example, is approx. 8 g/cm^3. The density of the composite C143-75, on the other hand, is only 1.71 g/cm^3, equivalent to a factor of 4.68. In order to include all aspects in a fair comparison between the composites and SS, simulations of the

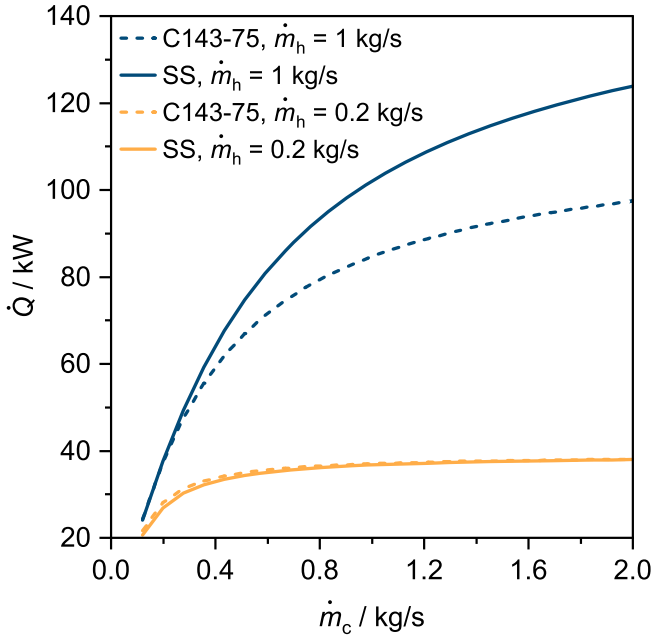

FIGURE 9 Simulated heat fluxes transferred by a PHE. $T_{c,in} = 30°C$, $T_{c,in} = 80°C$. $N_{p,C143\text{-}75} = 27$, $N_{p,SS} = 9$.

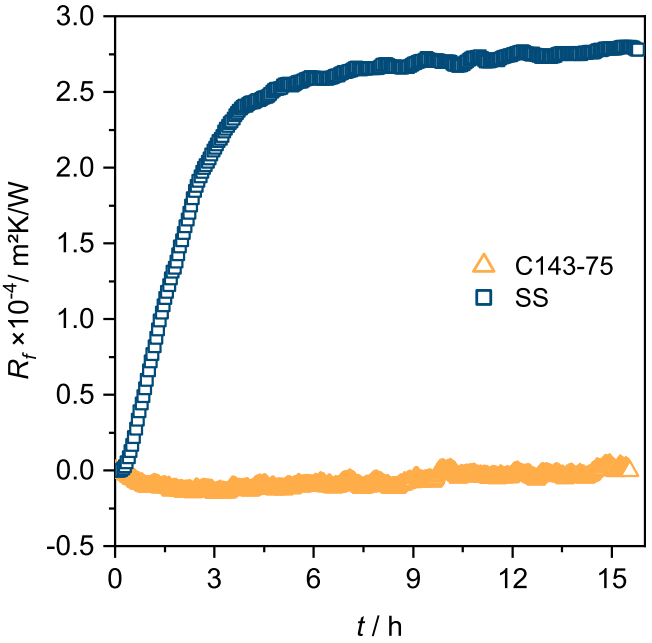

FIGURE 10 Thermal fouling resistances for $CaCO_3$ fouling. $T_{c,in} = 35°C$, $T_{h,in} = 90°C$. $b_{CaCO3} = 3.5$ mmol/kg. s = 1 mm.

transferred heat fluxes in a PHE were carried out being shown in Figure 9. To account for the density difference, the results for SS were calculated with nine thermal plates and for the composite C143-75 with 27 plates. In the direct material comparison, not the Reynolds numbers but the mass flow rates were kept constant, corresponding to the heating or cooling of a certain amount of fluid. If the curve of the composite is below that of SS, this is equivalent to the fact that a larger area (or larger PHE mass) is required for the same task and vice versa. Furthermore, wall thicknesses of 1 mm for SS and 1.5 mm for the composite are assumed to account for the poorer mechanical stability. The mass flows ($\dot{m}_c$ and $\dot{m}_h$, respectively) were chosen to cover a wide Reynolds number range with respect to SS ($Re_{SS} = 1000–6000$). Due to the higher number of plates and the consequently larger cross-sectional area flowed through, lower Reynolds numbers result for C143-75 at the same mass flows ($Re_{C143\text{-}75} = 350–2000$). It is evident that performance differences between the materials only become apparent at high mass flows (and consequently high Reynolds numbers) to the advantage of SS. For a mass flow of the hot fluid side of 0.2 kg/s ($Re_h = 1000$), there is practically no difference between the two materials. In this case, the convective heat transfer on the hot fluid side is the limiting factor. In the case of the highest investigated mass flows ($\dot{m}_h = 1$ kg/s and $\dot{m}_c = 2$ kg/s), there is a difference in simulated heat transfer of 27%.

Taking all influencing factors into account, it can be stated that the polymer composites, despite their quite low thermal conductivities compared to SS, can certainly provide high heat fluxes. Particularly in the field of highly corrosive media, they could thus represent a favorable alternative to the conventional expensive alloys.

3.3 | Fouling susceptibility

In many industrial processes, not only aging and corrosion of heat transfer materials occur, but also the formation of fouling layers, which can extremely reduce the performance of heat exchangers by the formation of an additional thermal resistance. This influence of crystallization fouling on the thermal performance of SS and the newly developed polymer composite C143-75 is shown below for the model salts calcium carbonate (Figure 10) and calcium sulfate (Figure 11). For both salt systems, significant advantages of the composite over SS can be seen.

In the case of the more dynamic $CaCO_3$ fouling (see Figure 10), asymptotic fouling resistances form after about 15 h of testing. Where an asymptotic fouling resistance of 0.27 m^2K/kW is formed on SS, the composite shows almost no fouling susceptibility. Consequently, this also applies to the fouling kinetics, which are expressed by the linear increase of the fouling resistance. Even if this is not evident in this plot, the fouling resistance related to C143-75 increases by 1.1E−3 m^2K/kW per hour from a testing time of 2 h. The fouling resistance of the SS sample, on the other hand, increases in the

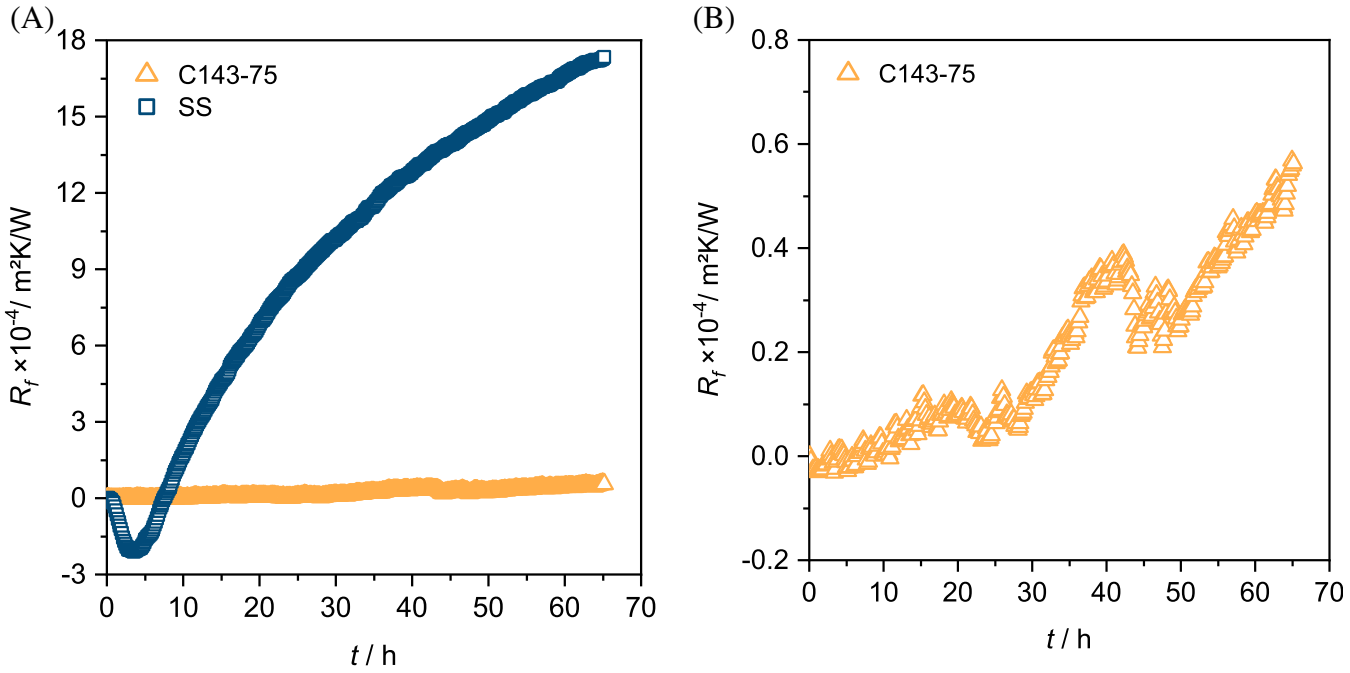

FIGURE 11 Thermal fouling resistances for $CaSO_4$ fouling. $T_{c,in} = 35°C$; $T_{h,in} = 90°C$; $b_{CaSO4} = 25$ mmol/kg; s = 1 mm. (A) SS and C143-75, (B) Detailed view of C143-75.

initial phase by 8.8E−2 m²K/kW per hour, which corresponds to a factor of 80. For $CaSO_4$ fouling, the quantitative difference between the developing thermal fouling resistances is even more pronounced as can be seen in Figure 11. A fouling resistance of 1.7 m²K/kW forms after more than 60 h, although the asymptotic fouling resistance has not yet been reached at this point. For comparison: the thermal resistance of the SS wall is 0.067 m²K/kW and that of the polymer composite wall is 0.625 m²K/kW. As a result, the initially lower U value of the polymer composite sample exceeds the value of the SS sample during the test duration. It is also noticeable, that at the beginning of the fouling test, a phase with negative fouling resistance occurs in the case of SS (a phenomenon, which could be observed by many authors[33-35]), whereas it does not in the case of C143-75. If negative fouling resistances are measured, the convective heat transfer is increased compared to the initial conditions. This increased heat transfer results from initial crystal formation on the surface. While these provide an additional thermal resistance, they also promote turbulences on the surface. However, when the salt crystals exceed a critical mass, the additional thermal resistance predominates ($t = 7$ h). There are two reasons why the phenomenon shown does not occur on the polymer composite surface. First, its surface is rougher, which is why the increase in convective heat transfer due to crystal formation is lower. And second, an improvement in convective heat transfer has less effect on the overall heat transfer because a larger part of the thermal resistance is located in the wall due to the lower thermal conductivity, compared to SS.

Taking fouling processes into account, the performance of the polymer composites investigated can exceed that of SS in terms of the transferred heat. Additionally, it must be noted that not completely identical conditions prevailed during the fouling tests. The boundary conditions were kept constant, but due to the lower thermal conductivity of C143-75 compared to SS, lower wall temperatures develop there, which significantly influence the fouling process. Higher wall temperatures during crystallization fouling of $CaSO_4$ and $CaCO_3$, lead to higher fouling rates due to higher supersaturations, which has already been shown in many studies. To put this into perspective, it must be added that higher process temperatures are difficult to realize with the composites developed due to their limited temperature stability. In order to transfer the same quantity of heat, the heat exchangers would have to be dimensioned larger compared to SS (increased heat transfer surface). A higher wall temperature resulting in a higher fouling rate is, therefore, unlikely. Possible properties underlying fouling-resistant surfaces have been discussed frequently in the literature.[36-39] In most cases, the topographical and energetic surface properties are used for evaluation, which are shown below for a selection of the materials investigated in Table 2 and Figure 12.

What should always be considered is that the mentioned properties can affect the measurement methods

TABLE 2 Mean arithmetic roughnesses S_a.

Material	S_a/µm
C143-75	0.76
C143-75-exp	1.31
C143-75-sb	9.79
C143-80	0.74
C145-80	0.7
C144-75	0.58
SS	0.08

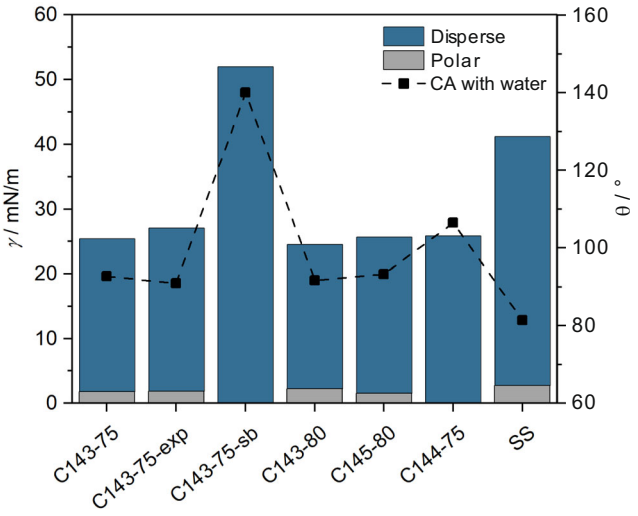

FIGURE 12 Surface free energies and static contact angles (CA) with water.

mutually. For example, the significant increase in roughness of the polymer composites by sandblasting (see Table 2) also results in significantly higher contact angles and surface free energies. However, Young's equation used to determine surface free energies, is only valid for perfectly smooth surfaces.[40] Yet an increase in roughness leads to an increase in the contact angle for liquids that have a contact angle >90° on the smooth surface and vice versa.[41] As a result, the sandblasting of the materials apparently increases the surface free energy. The actual value should be the same as that of the non-sandblasted sample. Furthermore, a separate evaluation, that is, which property contributes to which extent to more or less fouling, is hardly possible, since the two samples investigated have different surface energies and roughness. As shown in Table 2 and Figure 12, different PP grades and different graphite contents cause only minor differences in the properties considered. The sample C143-75 examined in the fouling tests can, therefore, be regarded as representative of the entire material class. Only the sandblasting of the materials causes a significant difference in the surface properties.

A high surface roughness, which usually results in a shorter induction phase due to faster nucleation processes, does not seem to be crucial for the fouling process with the investigated materials. The reason for this assumption is the many times higher roughness of the composite compared to SS. The advantage over SS in terms of lower asymptotic fouling resistance and slower crystallization fouling kinetics must therefore be due to the different surface free energies of the materials investigated. Overall, it can be stated that the polymer composite surfaces possess a lower surface energy than the SS surface, which in this particular case appears to lead to a lower susceptibility to fouling. The fact that a lower surface energy leads to less deposit formation is in accordance with the literature.[37,38,42,43] However, the different energetic behavior of different surfaces at the interface between the initial crystals and the surface is very complex and cannot be reduced to one parameter alone, such as the surface free energy.[44] Therefore, no correlation can be given between surface free energy and fouling behavior. Furthermore, it cannot be stated in general that the use of polymer surfaces always leads to reduced fouling susceptibility compared to metallic surfaces. Several authors have observed both an increase[45] and a decrease[43,46] in fouling susceptibility in a direct comparison of polymer surfaces with metallic surfaces. An assessment must, therefore, always be made in a direct comparison, whereby a low-surface energy seems generally to be preferred. This usually results also in poor adhesion of deposits,[39] which facilitates cleaning of the heat exchangers in place and may avoid blocking of single channels. For this reason, surface treatments and coatings that reduce the surface energy of thermal plates of PHEs have proven to be very useful.[36,38] The low adhesion forces between surface and crystal due to low energy surfaces can also be observed for the material C143-75 investigated here. This becomes obvious when taking a more detailed look at the fouling curves shown (see Figure 11). After about 40 h of testing, a sudden drop in the fouling curve occurs, caused by a part of the fouling layer flaking off. This self-cleaning effect could lead to consistently low fouling resistances and consequently longer service time intervals, especially when high shear forces and turbulence are generated (as is the case in PHEs). However, in order to transfer these positive results to PHEs, an optimal design (shape and size of the plates, overall flow design, etc.) of the unit is necessary.

4 | CONCLUSIONS

The present study shows, that the manufacturing of highly filled polypropylene/graphite composites can

compensate for many of the disadvantages of pure polymers for use in heat exchangers, which makes their use as thermal plates in PHEs conceivable. The addition of graphite to the PP matrix resulted in the required improvement in thermal as well as mechanical properties for the proposed application. Composite materials with 75 wt% graphite represented the best trade-off between mechanical and thermal properties. Higher loadings lead to a drop in mechanical properties with a comparatively small increase in thermal conductivity. The flexural modulus increased from 1.4 MPa to at least 7.6 MPa compared to pure PP, leading to a stiffer material required for use in PHEs. In addition, contact points in PHE between adjacent plates provide the necessary mechanical stability over a wide pressure range estimated at 7 bar differential pressure.

The process of sheet extrusion limits the effective thermal conductivity of the heat exchanger sheets due to an in-plane orientation of the anisotropic graphite particles, resulting in comparatively low thermal conductivities of a maximum of 2.74 W/mK. However, the low density of the developed compounds of a maximum of 1.78 g/cm^3, ensures the realization of large heat transfer surfaces at the same heat exchanger weight compared to metallic PHEs, largely compensating for their lower thermal conductivity, especially at low Reynolds numbers.

The low fouling susceptibility of the materials due to their low-surface energy makes their use particularly attractive in fouling-prone systems. Due to the lower thermal conductivity of the polymer composites, the use of stainless steel provides higher heat transfer rates, although this fact can be reversed by the formation of larger fouling layers on the metal, as was the case for the calcium sulfate model system studied. The fouling resistance on stainless steel in this case exceeded that on the composite with 75 wt% graphite by more than 20 times. In addition, the low adhesion of deposits to the composite materials leads to a self-cleaning effect that could reduce downtimes for cleaning in technical processes.

The PP-graphite compounds have excellent corrosion resistance at a low price compared to metallic alternatives which come with expensive raw materials and manufacturing processes. These positive characteristics already make the developed materials a suitable alternative to metallic materials in PHEs.

NOMENCLATURE

A	heat transfer surface, m
b	molality, mol/kg
a	corrugation amplitude, m
C	heat capacity flow rate, W/K
E_{flex}	flexural modulus, GPa
h	convective heat transfer coefficient, W/m^2 K
k	thermal conductivity, W/m K
L	effective heat exchanger length, m
$\dot{m}$	mass flow rate, kg/s
N_p	number of plates, –
P	corrugation pitch, m
Q	heat transfer rate, W
R_f	thermal fouling resistance, m^{2}K/W
Re	Reynolds number, –
s	wall thickness, m
S_a	mean arithmetic roughness, μm
t	time, h
T	temperature, °C
U	overall heat transfer coefficient, W/m^{2}K
w	effective heat exchanger width, m
x	length, m

Special characters

α	thermal diffusivity, mm^2/s
β	Chevron angle
γ	surface free energy, m
ε_{b}	strain at break, %
ΔT_{lm}	mean log temperature difference, K
Φ	enlargement factor, –
σ_{flex}	flexural strength, MPa
σ	stress, MPa
Θ	contact angle

Subscripts

0	initial conditions
1	fluid stream 1
2	fluid stream 2
c	cold
f	fouled surface
flex	flexural
h	hot
i	channel i
n	channel n
w	conditions at the wall

Abbreviations

CA	contact angle
PHE	plate heat exchanger
PP	polypropylene
SS	stainless steel

ACKNOWLEDGMENTS

The authors would like to thank the German Federation of Industrial Research Associations (AiF) and the German Federal Ministry for Economic Affairs and Climate Action for the financial support of the project (IGF-20999 N/1), which has been honored as best 2023 project

guided by GVT (Gesellschaft für Verfahrenstechnik, Frankfurt). Open Access funding enabled and organized by Projekt DEAL.

CONFLICT OF INTEREST STATEMENT

The authors declare no conflicts of interest.

DATA AVAILABILITY STATEMENT

The data that support the findings of this study are available from the first author (Hendrik Kiepfer) upon reasonable request.

ORCID

Hendrik Kiepfer https://orcid.org/0000-0003-1552-0386

REFERENCES

1. Kleme JJ, Arsenyeva O, Kapustenko P, Tovazhnyanskyy L. *Compact Heat Exchangers for Energy Transfer Intensification. Low Grade Heat and Fouling Mitigation*. CRC Press; 2016.
2. Bond MP. Plate heat exchangers for efficient heat transfer. *Chem Eng*. 1981;162.
3. Kerner J, Sjogren S, Svensson L. *Power*. Where plate exchangers offer advantages over shell-and-tube. 1987;131:53.
4. Kapustenko P, Boldyryev S, Arsenyeva O, Khavin G. The use of plate heat exchangers to improve energy efficiency in phosphoric acid production. *J Cleaner Prod*. 2009;17:951-958.
5. Zohuri B. In: Zohuri B, ed. *Compact Heat Exchangers*. Springer International Publishing; 2017:57-185.
6. Zhang J, Zhu X, Mondejar ME, Haglind F. A review of heat transfer enhancement techniques in plate heat exchangers. *Renew Sustain Energy Rev*. 2019;101:305-328.
7. Luckow P, Bar-Cohen A, Rodgers P, Cevallos J. Energy efficient polymers for gas-liquid heat exchangers. *J Energy Res Technol*. 2010;132:132.
8. Chen X, Su Y, Reay D, Riffat S. Recent research developments in polymer heat exchangers – A review. *Renew Sustain Energy Rev*. 2016;60:1367-1386.
9. T'Joen C, Park Y, Wang Q, Sommers A, Han X, Jacobi A. A review on polymer heat exchangers for HVAC&R applications. *Int J Refrig*. 2009;32:763-779.
10. Kakaç S, Liu H, Pramuanjaroenkij A. Heat exchangers. In: Kakaç, Liu H, Pramuanjaroenkij A, eds. *Selection, Rating, and Thermal Design*. CRC Press; 2020:471-497.
11. Song S, Zhang Y. Carbon nanotube/reduced graphene oxide hybrid for simultaneously enhancing the thermal conductivity and mechanical properties of styrene-butadiene rubber. *Carbon*. 2017;123:158-167.
12. Kim G-H, Lee D, Shanker A, et al. High thermal conductivity in amorphous polymer blends by engineered interchain interactions. *Nat Mater*. 2015;14:295-300.
13. Burger N, Laachachi A, Ferriol M, Lutz M, Toniazzo V, Ruch D. Review of thermal conductivity in composites: Mechanisms, parameters and theory. *Prog Polym Sci*. 2016;61:1-28.
14. Chen H, Ginzburg VV, Yang J, et al. Thermal conductivity of polymer-based composites: fundamentals and applications. *Prog Polym Sci*. 2016;59:41-85.
15. Ghaffari-Mosanenzadeh S, Aghababaei Tafreshi O, Dammen-Brower E, Rad E, Meysami M, Naguib HE. A review on high thermally conductive polymeric composites. *Polym Compos*. 2022;43:692-711.
16. Glade H, Moses D, Orth T. In: Bart H-J, Scholl S, eds. *Innovative Heat Exchangers*. Springer International Publishing; 2018:53-116.
17. Schilling S, Glade H, Orth T. Investigation of Crystallization Fouling on Novel Polymer Composite Heat Exchanger Tubes. *Heat Transfer Eng*. 2022;43:1326-1336.
18. Jamzad P, Kenna J, Bahrami M. Development of novel plate heat exchanger using natural graphite sheet. *Int J Heat Mass Transfer*. 2019;131:1205-1210.
19. Rzeczkowski P, Krause B, Pötschke P. Characterization of highly filled PP/graphite composites for adhesive joining in fuel cell applications. *Polymers*. 2019;11:11.
20. Steinhagen R, Müller-Steinhagen H, Maani K. Problems and costs due to heat exchanger fouling in New Zealand industries. *Heat Transfer Eng*. 1993;14:19-30.
21. Zettler HU. C3 Wärmeübertrager: Verminderung der Ablagerungsbildung. In: Stephan P, Kabelac S, Kind M, Mewes D, Schaber K, Wetzel T, eds. *VDI-Wärmeatlas*. Springer; 2019:99-134.
22. Ha SM, Lee HL, Lee S-G, et al. Thermal conductivity of graphite filled liquid crystal polymer composites and theoretical predictions. *Compos Sci Technol*. 2013;88:113-119.
23. Kaelble DH. Dispersion-polar surface tension properties of organic solids. *J Adhes*. 1970;2:66-81.
24. Owens DK, Wendt RC. Estimation of the surface free energy of polymers. *J Appl Polym Sci*. 1969;13:1741-1747.
25. Wanniarachchi AS, Ratnam U, Tilton BE, Dutta-Roy K. Proceedings of the 30th 1995 National Heat Transfer Conference. Paper Presented at: *The 1995 National Heat Transfer Conference*, Portland, Oregon, August 6–8, 1995, American Society of Mechanical Engineers, New York, NY, 1995.
26. Osswald TA, Baur E, Brinkmann S, Oberbach K, Schmachtenberg E. *International Plastics Handbook. The Resource for Plastics Engineers*. 4th ed. Hanser; 2006.
27. Ehrenstein GW. *Polymer-Werkstoffe. Struktur—Eigenschaften—Anwendung*. 3rd ed. Hanser; 2011.
28. Abu-Khader MM. Plate heat exchangers: Recent advances. *Renew Sustain Energy Rev*. 1883;2012:16.
29. Kada D, Koubaa A, Tabak G, Migneault S, Garnier B, Boudenne A. Tensile properties, thermal conductivity, and thermal stability of short carbon fiber reinforced polypropylene composites. *Polym Compos*. 2018;39:E664-E670.
30. Wang L. *Plate Heat Exchangers. Design, Applications and Performance*. Vol 11. WIT Press; 2007.
31. Kiepfer H, Stannek H, Kuypers M, Grundler M, Bart H-J, eds. Paper presented at: Proceedings of the 15th International Conference on Heat Transfer, Fluid Mechanics and Thermodynamics (HEFAT2021), ed. HEFAT; 2021, pp. 1174–1179.
32. Chung S-H, Kim H, Jeong SW. Improved thermal conductivity of carbon-based thermal interface materials by high-magnetic-field alignment. *Carbon*. 2018;140:24-29.
33. Bansal B, Müller-Steinhagen H, Chen XD. Performance of plate heat exchangers during calcium sulphate fouling—investigation with an in-line filter. *Chem Eng Process Process Intensif*. 2000;39:507-519.
34. Crittenden BD, Alderman NJ. Negative fouling resistances: the effect of surface roughness. *Chem Eng Sci*. 1988;43:829-838.
35. Dreiser C, Bart H-J. Mineral scale control in polymer film heat exchangers. *Appl Therm Eng*. 2014;65:524-529.

36. Barish JA, Goddard JM. Anti-fouling surface modified stainless steel for food processing. *Food Bioprod Process*. 2013;91:352-361.
37. Müller-Steinhagen H, Zhao Q, Helali-Zadeh A, Ren X-G. The effect of surface properties on CaSO4scale formation during convective heat transfer and subcooled flow boiling. *Can J Chem Eng*. 2000;78:12-20.
38. Zettler HU, Wei M, Zhao Q, Müller-Steinhagen H. Influence of surface properties and characteristics on fouling in plate heat exchangers. *Heat Transfer Eng*. 2005;26:3-17.
39. Zhao Q, Liu Y, Wang S. Surface modification of water treatment equipment for reducing CaSO4 scale formation. *Desalination*. 2005;180:133-138.
40. Zielke PC. PhD thesis, Friedrich-Alexander-Universität Erlangen-Nürnberg; 2008.
41. Quéré D. Wetting and roughness. *Annu Rev Mater Res*. 2008; 38:71-99.
42. Müller-Steinhagen H, Zhao Q. Paper presented at: *Proceedings of the 4th International Conference on Heat Exchanger Fouling: Fundamental Approaches & Technical Solutions*, Davos, Switzerland, July 8–13, 2001, ed. H. Müller-Steinhagen, Publico-Publ, Essen, 2002.
43. Kazi SN, Duffy GG, Chen XD. Mineral scale formation and mitigation on metals and a polymeric heat exchanger surface. *Appl Therm Eng*. 2010;30:2236-2242.
44. Geddert T, Augustin W, Scholl S. Induction time in crystallization fouling on heat transfer surfaces. *Chem Eng Technol*. 2011; 34:1303-1310.
45. Wu Z, Davidson JH, Francis LF. Effect of water chemistry on calcium carbonate deposition on metal and polymer surfaces. *J Colloid Interface Sci*. 2010;343:176-187.
46. Wu Z, Francis LF, Davidson JH. Scale formation on polypropylene and copper tubes in mildly supersaturated tap water. *Sol Energy*. 2009;83:636-645.

How to cite this article: Kiepfer H, Stannek P, Grundler M, Bart H-J. Thermally conductive polypropylene composites as corrosion-resistant materials for plate heat exchangers. *Polym Compos*. 2023;44(10):7002-7016. doi:10.1002/pc.27613